The Swarm Initial Field Model for the 2014 geomagnetic field

Nils Olsen[1], Gauthier Hulot[2], Vincent Lesur[3], Christopher C. Finlay[1], Ciaran Beggan[4], Arnaud Chulliat[5], Terence J. Sabaka[6], Rune Floberghagen[7], Eigil Friis-Christensen[1], Roger Haagmans[8], Stavros Kotsiaros[1], Hermann Lühr[3], Lars Tøffner-Clausen[1], and Pierre Vigneron[2]

[1]DTU Space, National Space Institute, Technical University of Denmark, Kongens Lyngby, Denmark, [2]Equipe de Géomagnétisme, Institut de Physique du Globe de Paris, Sorbonne Paris Cité, Université Paris Diderot, UMR 7154 CNRS/INSU, Paris, France, [3]Helmholtz-Zentrum Potsdam, Deutsches GeoForschungsZentrum, Potsdam, Germany, [4]British Geological Survey, Edinburgh, UK, [5]National Geophysical Data Center, NOAA, Boulder, Colorado, USA, [6]Planetary Geodynamics Branch, NASA GSFC, Greenbelt, Maryland, USA, [7]Directorate of Earth Observation Programmes, ESRIN, Frascati, Italy, [8]ESA/ESTEC, Noordwijk, Netherlands

Abstract Data from the first year of ESA's *Swarm* constellation mission are used to derive the Swarm Initial Field Model (SIFM), a new model of the Earth's magnetic field and its time variation. In addition to the conventional magnetic field observations provided by each of the three Swarm satellites, explicit advantage is taken of the constellation aspect by including east-west magnetic intensity gradient information from the lower satellite pair. Along-track differences in magnetic intensity provide further information concerning the north-south gradient. The SIFM static field shows excellent agreement (up to at least degree 60) with recent field models derived from CHAMP data, providing an initial validation of the quality of the Swarm magnetic measurements. Use of gradient data improves the determination of both the static field and its secular variation, with the mean misfit for east-west intensity differences between the lower satellite pair being only 0.12 nT.

1. Introduction

The three-satellite constellation mission *Swarm* was launched by the European Space Agency (ESA) on 22 November 2013. Swarm consists of three identical spacecraft, two of which (*Swarm Alpha*, in following denoted as SW-A, and *Swarm Charlie*, SW-C) are flying almost side by side in polar orbits (of inclination 87.4°) at lower altitude (about 465 km above a mean radius of $a = 6371.2$ km in January 2015). The east-west separation of their orbits is 1.4° in longitude corresponding to 155 km at the equator. The third satellite, *Swarm Bravo* (SW-B) is in a slightly higher (about 520 km altitude in January 2015) orbit of inclination 88°. Each of the three satellites carries an **A**bsolute **S**calar **M**agnetometer (ASM) for measuring Earth's magnetic field intensity, a **V**ector **F**luxgate **M**agnetometer (VFM) measuring the direction and strength of the magnetic field, and a three-head Star Tracker mounted close to the VFM to obtain the attitude needed to transform the vector readings to a known coordinate frame. Time and position are provided by onboard GPS. The payload also includes instruments to measure plasma and electric field parameters as well as gravitational acceleration. More information about the mission after 1 year in space can be found in R. Floberghagen et al. (The Swarm mission—An overview one year after launch, submitted to *Earth, Planets and Space*, 2015). All Swarm data are available at http://earth.esa.int/swarm.

This paper describes a model of the Earth's magnetic field that has been derived from the first year of Swarm magnetic data. For this model we use observations of the magnetic field intensity and direction as well as information on the horizontal gradient of the magnetic field. Approximations of the north-south (N-S) gradient are obtained from along-track differences of intensity measurements at each of the three satellites following an approach that has recently been applied to data from the CHAMP satellite [*Kotsiaros et al.*, 2015; *Sabaka et al.*, 2015]. In addition, and for the first time in geomagnetic field modeling, we also use estimates of the east-west (E-W) field gradient by taking the difference of the magnetic field intensity measured by the lower Swarm satellite pair, SW-A and SW-C.
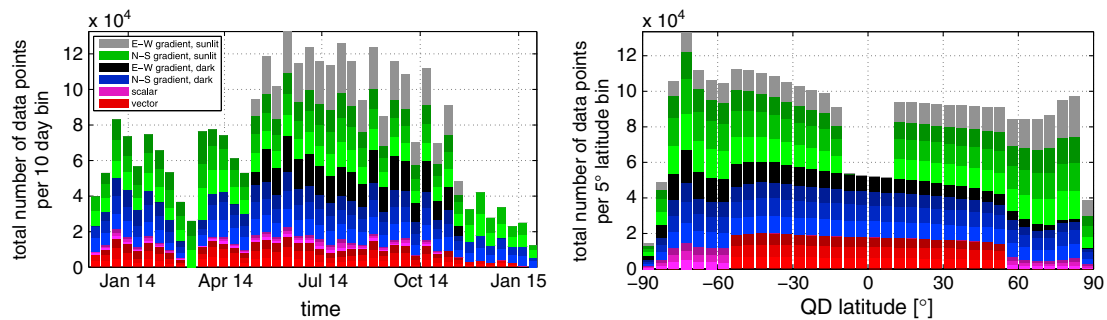
Figure 1. Total number of Swarm satellite data (stacked histogram) as a function of (left) time and (right) latitude, respectively. For vector (red), scalar (purple), and N-S gradient (blue and green) data, the dark/normal/light color represents SW-A/SW-B/SW-C. E-W gradient data are shown in black and grey.

2. Data Selection and Model Parameterization

We used nearly 14 months (26 November 2013 to 17 January 2015) of magnetic data from the three Swarm satellites. Nightside data during geomagnetically quiet times, downsampled to 30 s by taking one data point in 30 from the 1 Hz Level 1b-data (version 0302 when available, otherwise version 0301), have been selected using the same criteria as for the CHAOS-4 model [*Olsen et al.*, 2014]. In particular, we select data (vector and scalar) from dark regions only (Sun at least 10° below the horizon) for which the strength of the magnetospheric ring-current, estimated using the *RC* index [*Olsen et al.*, 2014], changed by at most 2 nT/h. At quasi-dipole (QD) latitudes [*Richmond*, 1995] equatorward of ±55°, we require that the geomagnetic activity index $Kp \leq 2°$, while for regions poleward of 55° QD latitude the weighted average over the preceding 1 h of the merging electric field at the magnetopause [e.g., *Kan and Lee*, 1979; *Newell et al.*, 2007] has to be below 0.8 mV/m.

Three vector components of the magnetic field were taken for nonpolar latitudes (equatorward of ±55° QD latitude), while only scalar data were used for higher latitudes. Each vector measurement of the VFM $\mathbf{B}_{VFM}$ has been normalized such that its intensity is equal to that measured by the ASM: $|\mathbf{B}_{VFM}| = F_{ASM}$.

In addition to these data of the magnetic field, we include horizontal difference data ("gradient data") of magnetic intensity *F*. In contrast to the selection of magnetic vector and scalar field data ($Kp \leq 2^0$, $|dRC/dt| < 2$ nT/h, a condition that is fulfilled for 27% of the time), we allow for higher geomagnetic activity when selecting gradient data ($Kp < 3^0$, $|dRC/dt| < 3$ nT/h, which is fulfilled for 45% of the time) and also use gradient data from the dayside. We choose to exclude dayside data at QD latitudes $< \pm 10°$ to avoid contamination by the equatorial electrojet.

In order to approximate the east-west gradient, we took the difference of scalar intensity data, $\delta F_{EW} = \pm[F_A(t_1, r_1, \theta_1, \phi_1) - F_C(t_2, r_2, \theta_2, \phi_2)]$, measured by the two satellites SW-A and SW-C. Here $t_i, r_i, \theta_i, \phi_i, i = 1$–2 are time, radius, geographic colatitude, and longitude of the two observations. The sign of the difference was chosen such that $\delta\phi = \phi_1 - \phi_2 > 0$. We do not divide the field differences by the spatial distance between the observations to obtain a spatial gradient with units nT/km, because we prefer to work with magnetic field differences with units nanotesla. For each scalar observation F_A (from SW-A) fulfilling the above selection criteria, we selected the corresponding value F_C (from SW-C) that was closest in colatitude θ, with the additional requirement that $|\delta t| = |t_1 - t_2| < 50$ s.

The north-south gradient is approximated by the difference $\delta F_{NS} = \pm[F_k(t_k, r_k, \theta_k, \phi_k) - F_k(t_k + 15 \text{ s}, r_k + \delta r, \theta_k + \delta\theta, \phi_k + \delta\phi)]$ of subsequent scalar data measured by the same satellite ($k = 1, 2, \text{ or } 3$) 15 s later, corresponding to an along-track distance of ≈ 115 km ($\approx 1°$ in latitude near the equator). The sign of the difference was chosen positive if $\delta\theta > 0$, otherwise negative. We have only used scalar gradient data since the treatment of vector gradient data is much more demanding, in particular due to the "VFM-ASM disturbance field" that is presently under investigation.

Histograms of the data distribution in time and latitude are presented in Figure 1. E-W gradient data (shown in black/grey) are not available before April 2014 because the two satellites SW-A and SW-C have been flying in their nominal constellation (side by side) only since 18 April 2014. Exclusion of dayside near-equatorial gradient data is the reason for the decrease in the number of data at $< \pm 10°$ QD latitude.

All data are weighted proportional to $\sin\theta$ to simulate an equal-area distribution. Anisotropic magnetic errors due to attitude uncertainty [e.g., *Holme and Bloxham*, 1996] are considered assuming an error in the scalar intensity of $\sigma_F = 2$ nT and an isotropic attitude error of 5 arcsec. The value of $\sigma_F = 2$ nT is considerably higher than the measurement uncertainty of ≈ 0.2 nT because it also includes errors introduced by unmodeled magnetic field sources, mainly of external origin. However, since these external fields are rather large scale and cancel out when taking differences of nearby measurements, we are able to adopt an a priori data error of $\sigma_{\delta F} = 0.2$ nT for the magnetic field differences (i.e., the gradient data).

The model parameterization follows closely that of CHAOS-4. It consists of spherical harmonic expansion coefficients describing the magnetic field vector in an *Earth-Centered Earth-Fixed (ECEF)* coordinate system and sets of Euler angles needed to rotate the satellite vector readings from the magnetometer frame to the star tracker frame. The magnetic field vector in the ECEF frame, $\mathbf{B} = -\nabla V$, is derived from a magnetic scalar potential $V = V^{\text{int}} + V^{\text{ext}}$ consisting of a part, V^{int}, describing internal (core and lithospheric) sources, and a part, V^{ext}, describing external (mainly magnetospheric) sources and their Earth-induced counterparts. Both parts are expanded in terms of spherical harmonics.

For the internal part this yields

$$V^{\text{int}} = a \sum_{n=1}^{N_{\text{int}}} \sum_{m=0}^{n} \left(g_n^m \cos m\phi + h_n^m \sin m\phi \right) \left(\frac{a}{r} \right)^{n+1} P_n^m (\cos\theta) \tag{1}$$

where (r, θ, ϕ) are geographic coordinates, P_n^m are the associated Schmidt seminormalized Legendre functions, $\left\{ g_n^m, h_n^m \right\}$ are the Gauss coefficients describing internal sources, and $N_{\text{int}} = 70$ is the maximum degree and order of the internal expansion. Coefficients up to degree $n = 13$ include a linear dependence on time (linear secular variation). This yields $70 \times 72 + 13 \times 15 = 5235$ coefficients describing the internal part of Earth's magnetic field.

The external part of the field model is identical to that of CHAOS-4, with an expansion of the near magnetospheric sources (magnetospheric ring current) in the *Solar Magnetic (SM)* coordinate system (up to $n = 2$, with special treatment of the $n = 1$ terms) and of remote magnetospheric sources (e.g., magnetotail and magnetopause currents) in *Geocentric Solar Magnetospheric* coordinates (also up to $n = 2$ but restricted to order $m = 0$). We solve for an *RC* baseline correction (described by SM dipole coefficients that explicitly vary in time) in bins of 5 days (for $m = 0$) and 30 days (for $m = 1$), respectively, which in total results in 118 parameters describing the external field part of the model. See section 3 of *Olsen et al.* [2014] for details.

As part of the model estimation we solve for the Euler angles describing the rotation between the vector magnetometer frame and the star tracker frame in bins of 10 days (i.e., 3×41, 40 and 35 sets of angles for satellites Alpha, Bravo, and Charlie, respectively, resulting in an additional 348 model parameters).

The 5701 model parameters are estimated from approximately 4×10^6 observations (105,775 scalar data, $3 \times 394,218 = 1,182,654$ vector data, and 2,680,668 estimates of scalar gradients) by means of a regularized *Iteratively Reweighted Least Squares* approach using Huber weights. The gradient data were handled in a manner similar to that described in *Kotsiaros et al.* [2015] by taking the difference of the design matrices corresponding to the two positions $t_i, r_i, \theta_i, \phi_i, i = 1\text{--}2$. Gradient dayside data do not contribute to the core field part of the model (i.e., internal Gauss coefficients up to $n = 13$), whereas the remaining parts of the model are constrained by all data. No model regularization has been applied.

3. Results and Discussion

Table 1 lists the number of data points, together with means and root-mean-squared (RMS) misfit values between the observations and the predictions of the *Swarm Initial Field Model* (SIFM) model. At nonpolar latitudes the RMS misfit to the radial component B_r is below 2 nT, demonstrating the excellent quality of the *Swarm* magnetic field data. The RMS misfit of scalar intensity F and of the horizontal components is slightly higher, probably due to the impact of remaining unmodeled contributions from magnetospheric currents. Even more remarkable is the RMS misfit of the gradient data which (for dark conditions) is below 0.2 nT for the N-S gradient (obtained using data from the same instrument) and below 0.3 nT when looking at the difference between SW-A and SW-C. The nonzero mean value of -0.12 nT for the nonpolar, dark δF_{EW} is indicative of a very small relative offset between the two instruments, which is well within the expected

Table 1. Number N of Data Points, (Huber-Weighted) Mean, and RMS Misfit (in nT) of Scalar (F), Vector (B_r, B_θ, B_ϕ), N-S Gradient (δF_{NS}), and E-W Gradient (δF_{EW}) Data, at Polar ($> \pm 55°$) and Nonpolar ($< \pm 55°$) QD Latitudes

|	SW-A			SW-B			SW-C			SW-A − SW-C		
	N	Mean	RMS	N	Mean	RMS	N	Mean	RMS	N	Mean	RMS
F_{polar}	35,606	−0.27	3.47	36,387	−0.15	3.45	33,782	−0.13	3.45			
$F_{nonpolar}$	137,164	0.04	2.49	136,259	0.02	2.48	120,795	0.06	2.51			
B_r	137,164	0.00	1.97	136,259	−0.02	2.04	120,795	0.04	1.95			
B_θ	137,164	−0.13	3.23	136,259	−0.12	3.33	120,795	−0.20	3.31			
B_ϕ	137,164	−0.03	2.52	136,259	−0.05	2.52	120,795	−0.03	2.48			
$\delta F_{NS,polar}$	285,484	−0.01	1.12	287,940	−0.01	1.05	236,417	−0.02	1.06			
$\delta F_{NS,nonpolar,dark}$	198,626	0.00	0.19	198,955	0.00	0.18	167,801	0.00	0.18			
$\delta F_{NS,nonpolar,sunlit}$	217,910	0.02	0.34	219,557	0.02	0.32	176,916	0.01	0.33			
$\delta F_{EW,polar}$										279,777	−0.12	0.54
$\delta F_{EW,nonpolar,dark}$										197,769	−0.12	0.28
$\delta F_{EW,nonpolar,sunlit}$										211,152	−0.03	0.44

instrumental error budget of 0.3 nT. The dayside RMS misfits are slightly higher due to enhanced ionospheric contributions.

Figure 2a shows Mauersberger-Lowes spectra of the static (lithospheric) field part of the SIFM model and of analogous models derived from various data subsets: SIFM$_{no\ gradient}$, which was derived from vector and scalar intensity data without including gradient data; SIFM$_{NS\ gradient}$, which also included N-S gradient but no E-W gradient data; and SIFM$_{EW\ gradient}$, similar but including E-W gradient and no N-S gradient data. For reference we also present spectra from the MF7 [*Maus*, 2010] and CHAOS-4 [*Olsen et al.*, 2014] lithospheric field models, both derived mainly from CHAMP satellite data and not using any Swarm data.

Excluding gradient data (model SIFM$_{no\ gradient}$) leads to a lithospheric field model very similar to that of MF7 and CHAOS-4 up to degree $n = 40$, but with considerably more power above that degree (see dashed red curve). Including gradient data to build model SIFM reduces this power, making this model likely reliable up to at least $n = 60$ (see blue-dashed curve). This is also confirmed by the degree correlation of the various intermediate SIFM models with respect to MF7 (shown in Figure 2c). Note in particular the crucial improvement brought by the inclusion of the innovative E-W gradient data.

Figures 2e–2h present the relative difference between each coefficient of the different SIFM versions and MF7 in a degree versus order matrix and show that it is primarily high-degree coefficients that are modified when gradient data are included. A model built only from field data shows significant differences with respect to MF7 (Figure 2e), whereas inclusion of gradient data results in much better agreement (Figure 2h). In particular, N-S gradient data improve the determination of high-degree near-zonal coefficients ($|m| \approx 0 \ll n$), while E-W gradient data improve the near-sectorial terms ($|m| \approx n \gg 0$). There are, however, systematic differences between SIFM and MF7 in the sectorial terms above $n = 45$. This is likely due to a Backus effect [e.g., *Backus*, 1970; *Stern and Bredekamp*, 1975]. High-degree lithospheric field coefficients (above $n = 45$ or so) are primarily constrained by scalar gradient data, but these do not provide information concerning the small-scale details of the location of the dip equator, which is necessary to avoid this effect [*Khokhlov et al.*, 1997; *Ultré-Guérard et al.*, 1998]. This mainly affects the tesseral coefficients g_n^n, h_n^n and leads to models that are erroneous near the dip equator. Indeed, when looking at the difference in B_r between SIFM and MF7 the largest deviations occur in that region (Figure 3, right). In spite of this, the agreement between the two models is noteworthy, with an RMS vector field difference of only 7.5 nT (reduced to 6.9 nT when excluding QD latitudes $< \pm 10°$). Inclusion of more vector data will certainly help to reduce the Backus effect.

In addition to the static field, the secular variation (SV) also benefits from the inclusion of gradient information. This is apparent from comparisons of the SV (for epoch 2014.5) predicted by the SIFM and the CHAOS-5 model (C. C. Finlay et al., DTU candidate field models for IGRF-12 and the CHAOS-5 geomagnetic field model, submitted to *Earth, Planets and Space*, 2015) which was derived from a combination of Ørsted, CHAMP, SAC-C, Swarm, and ground observatory data (Figure 2b). Some care is needed with this comparison,
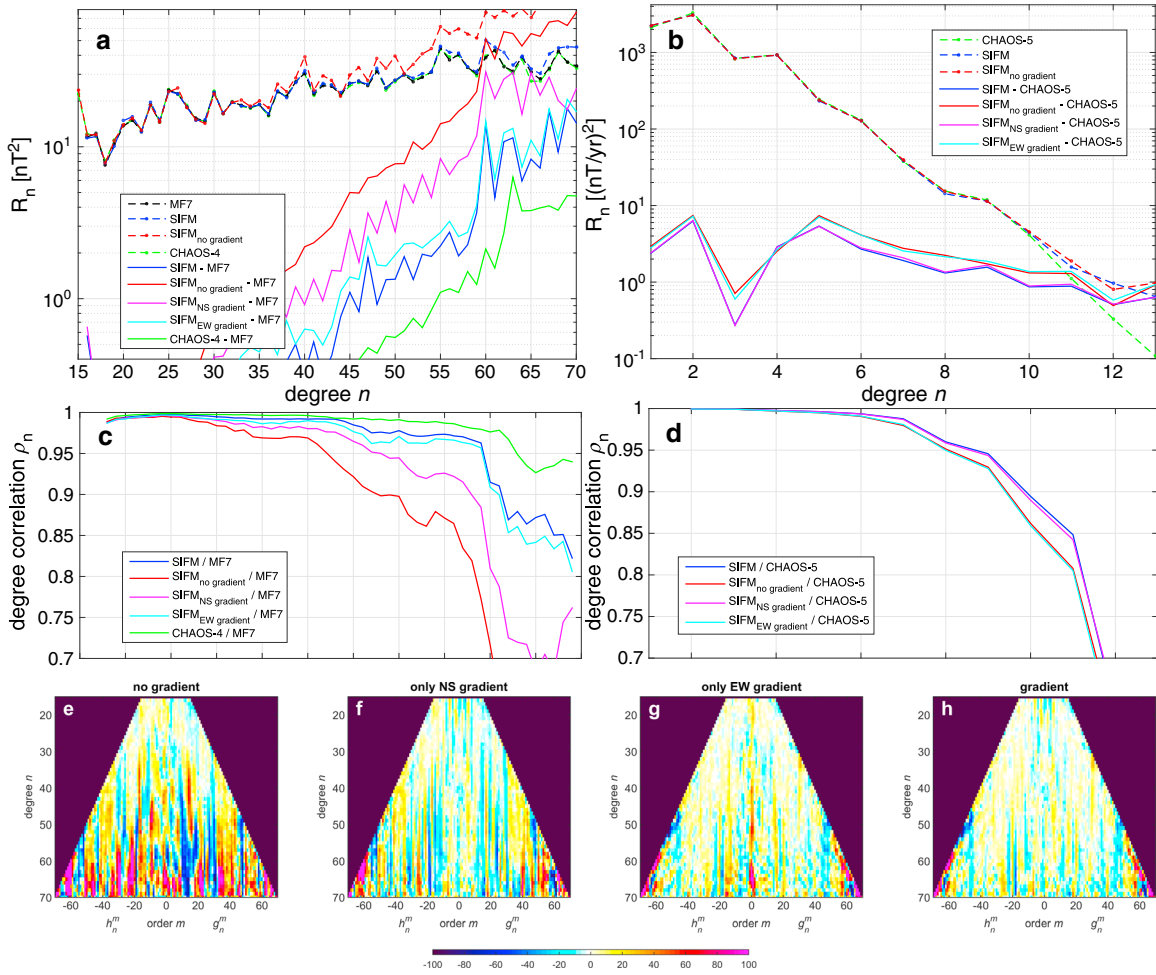
Figure 2. Lowes-Mauersberger power spectra (a) of the static field ($n = 15 - 70$) and (b) of the linear SV ($n = 1 - 13$) from the SIFM together with various reference and data subset model at the Earth's surface. Spectra of models are shown in dotted lines, spectra of differences between models in solid lines. Degree correlations of the SIFM and other models (c) with respect to model MF7 for the static field and (d) with respect to CHAOS-5 for the SV. Normalized coefficient differences (in %) with respect to MF7, for (e) SIFM$_{no\ gradient}$, (f) SIFM$_{NSgradient}$, (g) SIFM$_{EWgradient}$, and (h) SIFM, respectively.
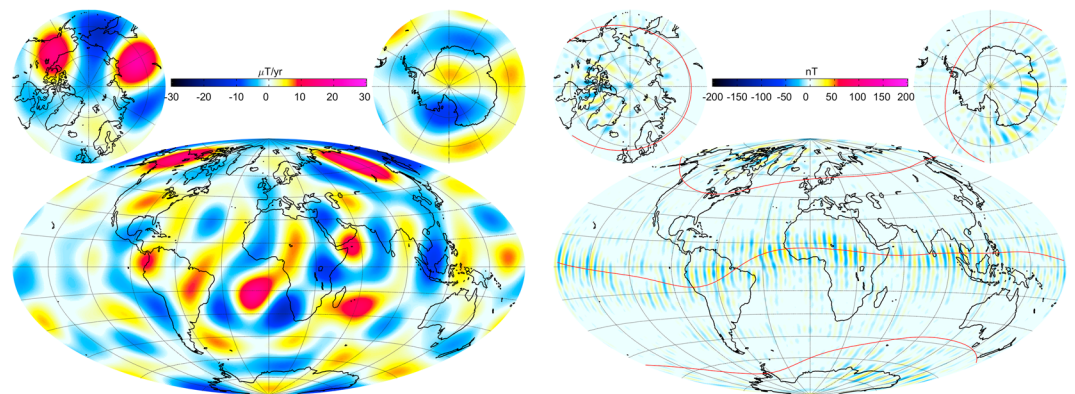
Figure 3. (left) November 2013 to January 2015 rate of change of B_r at the CMB from SIFM for degrees $n = 1 - 11$. (right) Difference of B_r at Earth's surface between SIFM and MF7, for degrees $n = 16 - 65$. Red lines locate the dip equator (0° QD latitude) and ±55° iso-QD latitudes.
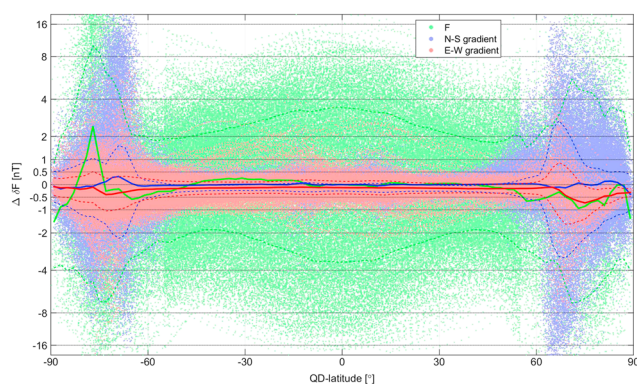
Figure 4. Residuals of the scalar (green) and scalar gradient (blue for N-S and red for E-W) data versus QD latitude for dark regions and magnetically quiet conditions. Note the nonlinear y axis ($\propto \arctan(y/5\ \mathrm{nT})$), which emphasizes near-zero values. Solid curves show the (Huber-weighted) mean value of the residuals in bins of 2° in latitude; dashed curves represent the mean ±1 standard deviation.

since CHAOS-5 was derived using a temporal smoothing that increased with spherical harmonic degree, while the SIFM provides an estimate of the SV time-averaged over the year for which Swarm data are available. Nevertheless, the SIFM SV agrees better with the CHAOS-5 SV than does the SIFM$_{\mathrm{nogradient}}$ SV. Interestingly, this improvement arises mainly due to the inclusion of the N-S gradient data, which appear to be efficient at removing magnetospheric contamination of the zonal terms of the modeled SV. These results are extremely encouraging, as they show that Swarm is already able to resolve yearly snapshots of the SV up to approximately $n = 11$. Figure 3 (left) shows a map of the rate of change that occurred in B_r between November 2013 and January 2015 at the core-mantle boundary (CMB), as predicted from the SIFM SV up to $n = 11$.

The ability of gradient data to enhance the resolution of the SIFM is impressive. It is interesting, in this respect, to have a close inspection of residuals (data minus SIFM predictions) in the scalar data F, N-S scalar differences δF_{NS}, and E-W differences δF_{EW}, for dark regions and quiet conditions ($Kp < 2$, $|dRC/dt| \leq 2$ nT/h, Figure 4). As expected, the largest residuals occur in the auroral zone (QD latitudes between ±65° and ±80°) and are primarily a result of polar electrojet activity. In contrast, residuals within the polar cap (> ±85°) and at nonpolar latitudes (< ±55°) are generally much smaller. Residuals in F, on the other hand, display much larger RMS misfits even at nonpolar latitudes, ranging from 2 nT (near QD latitudes of ±35°) up to 4 nT (near the dip equator). This is a clear signature of unmodeled contributions from the magnetospheric ring-current signal, which has a greater impact on F near the equator than at QD latitudes of ±35°. This rapidly varying magnetospheric signal effectively behaves as a source of noise in F. Fortunately, it also is very large scale, and thus, it affects gradient data (based on quasi-synchronous data, recall section 2) much less. This is the reason that gradient data are able to help improve the quality of the field model, validating the gradient component of the Swarm constellation concept.

4. Conclusion and Perspectives

After 1 year in space, the Swarm mission has provided a wealth of valuable data. Despite calibration issues that currently limit a full use of the constellation configuration advantages (see R. Floberghagen et al., submitted manuscript, 2015), these data can already be used to produce extremely impressive results. The SIFM model presented here provides a clear illustration of what can already be achieved.

Perhaps most importantly, the SIFM model is able to provide a description of the static lithospheric field that is remarkably close to that of the MF7 [*Maus*, 2010] and CHAOS-4 [*Olsen et al.*, 2014] models, up to at least degree and order 60, despite the fact that these earlier models did not use a single Swarm data and relied primarily on CHAMP data. This agreement provides both an initial validation of the Swarm mission and a valuable a posteriori validation of the CHAMP mission.

The SIFM model also provides an initial validation of the gradient concept underlying the Swarm mission [*Friis-Christensen et al.*, 2006]. Although not yet capable of achieving what could possibly be achieved when including low-altitude data from later mission phases [*Olsen et al.*, 2006], gradient data appear to be a very efficient way of increasing the resolution of geomagnetic field models.

More generally, the quality of the SIFM model is an encouraging preliminary result with regard to the core field and lithospheric field models [*Rother et al.*, 2013; *Sabaka et al.*, 2013; *Thébault et al.*, 2013] to be built and distributed by ESA as so-called L2 products of the mission [see *Olsen et al.*, 2013].

Finally, the demonstration that SV estimates up to $n = 11$ with a temporal resolution of 1 year can be built from Swarm data confirms that another important mission goal is within sight. The ability to study core field changes with high temporal resolution promises fresh insights on short-timescale core dynamics [see *Finlay et al.*, 2010], in particular regarding so-called geomagnetic jerks [*Mandea et al.*, 2010], pulses [*Chulliat et al.*, 2010], and fast torsional waves [*Gillet et al.*, 2010; *Silva et al.*, 2012].

Model coefficients and data sets used are available in different formats at www.spacecenter.dk/files/magnetic-models/SIFM/.

References

Backus, G. E. (1970), Non-uniqueness of the external geomagnetic field determined by surface intensity measurements, *J. Geophys. Res.*, *75*(31), 6339–6341.

Chulliat, A., E. Thébault, and G. Hulot (2010), Core field acceleration pulse as a common cause of the 2003 and 2007 geomagnetic jerks, *Geophys. Res. Lett.*, *37*, L07301, doi:10.1029/2009GL042019.

Finlay, C. C., M. Dumberry, A. Chulliat, and A. Pais (2010), Short timescale core dynamics: Theory and observations, *Space Sci. Rev.*, *155*, 177–218, doi:10.1007/s11214-010-9691-6.

Friis-Christensen, E., H. Lühr, and G. Hulot (2006), *Swarm*: A constellation to study the Earth's magnetic field, *Earth Planets Space*, *58*, 351–358.

Gillet, N., D. Jault, E. Canet, and A. Fournier (2010), Fast torsional waves and strong magnetic field within the Earth's core, *Nature*, *465*, 74–77, doi:10.1038/nature09010.

Holme, R., and J. Bloxham (1996), The treatment of attitude errors in satellite geomagnetic data, *Phys. Earth Planet. Int.*, *98*, 221–233.

Kan, J. R., and L. C. Lee (1979), Energy coupling function and solar wind-magnetosphere dynamo, *Geophys. Res. Lett.*, *6*, 577–580.

Khokhlov, A., G. Hulot, and J. Le Mouël (1997), On the Backus effect - I, *Geophys. J. Int.*, *130*, 701–703.

Kotsiaros, S., C. C. Finlay, and N. Olsen (2015), Use of along-track magnetic field differences in lithospheric field modelling, *Geophys. J. Int.*, *200*(2), 878–887, doi:10.1093/gji/ggu431.

Mandea, M., R. Holme, A. Pais, K. Pinheiro, A. Jackson, and G. Verbanac (2010), Geomagnetic jerks: Rapid core field variations and core dynamics, *Space Sci. Rev.*, *155*, 147–175, doi:10.1007/s11214-010-9663-x.

Maus, S. (2010), *Magnetic Field Model MF7*, CIRES, Colo. [Available at www.geomag.us/models/MF7.html.]

Newell, P. T., T. Sotirelis, K. Liou, C.-I. Meng, and F. J. Rich (2007), A nearly universal solar wind-magnetosphere coupling function inferred from 10 magnetospheric state variables, *J. Geophys. Res.*, *112*, A01206, doi:10.1029/2006JA012015.

Olsen, N., R. Haagmans, T. J. Sabaka, A. V. Kuvshinov, S. Maus, M. E. Purucker, V. Lesur, M. Rother, and M. Mandea (2006), The Swarm End-To-End mission simulator study: Separation of the various contributions to Earth's magnetic field using synthetic data, *Earth Planets Space*, *58*, 359–370.

Olsen, N., et al. (2013), The Swarm Satellite Constellation Application and Research Facility (SCARF) and Swarm data products, *Earth, Planets and Space*, *65*, 1189–1200.

Olsen, N., H. Lühr, C. C. Finlay, T. J. Sabaka, I. Michaelis, J. Rauberg, and L. Tøffner-Clausen (2014), The CHAOS-4 geomagnetic field model, *Geophys. J. Int.*, *197*, 815–827.

Richmond, A. D. (1995), Ionospheric electrodynamics using magnetic Apex coordinates, *J. Geomagn. Geoelectr.*, *47*, 191–212.

Rother, M., V. Lesur, and R. Schachtschneider (2013), An algorithm for deriving core magnetic field models from the Swarm data set, *Earth Planets Space*, *65*, 1223–1231.

Sabaka, T. J., L. Tøffner-Clausen, and N. Olsen (2013), Use of the Comprehensive Inversion Method for Swarm satellite data analysis, *Earth Planets Space*, *65*, 1201–1222.

Sabaka, T. J., N. Olsen, R. H. Tyler, and A. Kuvshinov (2015), CM5, a pre-*Swarm* comprehensive magnetic field model derived from over 12 years of CHAMP, Ørsted, SAC-C and observatory data, *Geophys. J. Int.*, *200*, 1596–1626.

Silva, L., L. Jackson, and J. Mound (2012), Assessing the importance and expression of the 6 year geomagnetic oscillation, *J. Geophys. Res.*, *117*, B10101, doi:10.1029/2012JB009405.

Stern, D. P., and J. H. Bredekamp (1975), Error enhancement in geomagnetic models derived from scalar data, *J. Geophys. Res.*, *80*, 1776–1782.

Thébault, E., P. Vigneron, S. Maus, A. Chulliat, O. Sirol, and G. Hulot (2013), Swarm SCARF Dedicated Lithospheric Field Inversion chain, *Earth Planets Space*, *65*, 1257–1270.

Ultré-Guérard, P., M. Hamoudi, and G. Hulot (1998), Reducing the Backus effect given some knowledge of the dip-equator, *Geophys. Res. Lett.*, *25*(16), 3201–3204, doi:10.1029/98GL02211.